The spectral function of the ω meson in nuclear matter from a coupled-channel resonance model*

P. Muehlich,† V. Shklyar, S. Leupold, U. Mosel, and M. Post

Institut für Theoretische Physik, Universität Giessen, D–35392 Giessen, Germany

Abstract

We calculate the spectral function of the ω meson in nuclear matter at zero temperature by means of the low-density theorem. The ωN forward scattering amplitude is calculated within a unitary coupled-channel effective Lagrangian model that has been applied successfully to the combined analysis of pion- and photon-induced reactions. While the peak of the ω spectral distribution is shifted only slightly, we find a considerable broadening of the ω meson due to resonance-hole excitations. For ω mesons at rest with respect to the surrounding nuclear medium, we find an additional width of about 60 MeV at saturation density.

PACS numbers: 14.40.Cs, 11.80.-m, 13.30.Eg, 13.85.Dz

Keywords: Properties of vector mesons, Relativistic scattering theory, Hadronic decays, Elastic scattering

*Supported by DFG

†Electronic address: pascal.muehlich@theo.physik.uni-giessen.de

I. INTRODUCTION

In the past years substantial theoretical and experimental effort has been directed to the search for modifications of hadrons embedded in a strongly interacting environment. These investigations have been driven by the expectation to gather information about one of the most exciting aspects of quantum chromodynamics (QCD), namely the restoration of the spontaneously broken chiral symmetry at finite temperatures and densities. The scalar quark condensate $\langle\bar{q}q\rangle$, which plays the role of an order parameter of the symmetry breaking mechanism and which develops a non-vanishing expectation value in vacuum, is expected to change from its vacuum value by roughly 30% already at normal nuclear matter density $\rho_0 = 0.16$ fm^{-3} [1, 2, 3, 4]. The prediction of dropping hadron masses in the nuclear medium driven by the chiral quark condensate in [5, 6] has therefore initiated a wealth of experiments searching for these changes in various kinds of nuclear reactions. In this respect, the light vector mesons play a central role as they couple directly to virtual photons. The latter can decay to dileptons which leave the strongly interacting system untouched, hence carrying information about the properties of the decayed vector mesons to the detectors without experiencing further interactions.

One approach which aims at a connection between hadronic properties and their in-medium modifications on one hand and non-perturbative quark and gluon condensates and their in-medium changes on the other is provided by the QCD sum rule approach. Originally the sum rules were introduced for the vacuum [7] but later on generalized to in-medium situations [8]. Concerning vector mesons it turned out that their in-medium changes are not directly connected to changes of the two-quark condensate, but to specific moments of the nucleon structure function and to changes of the four-quark condensate [6]. One might even turn the argument around and state that a measurement of modified vector meson spectra might give information on the density dependence of certain four-quark condensates rather than on the genuine chiral condensate $\langle\bar{q}q\rangle$ [9, 10]. Concerning the possible connection of four- and two-quark condensates see also [11]. In addition, it is important to stress that the sum rule approach does not directly constrain specific properties of a hadron like e.g. its mass. It constrains instead specific integrals over the spectral (vacuum or in-medium) information. For example, for the ρ-meson one can deduce from sum rules only that in a nuclear medium its spectral strength is shifted to lower invariant masses. Whether this shift is realized by a

mass shift [6], by an enlarged width [12, 13] or by the excitation of low-lying resonance-hole pairs [14] cannot be decided from a sum rule analysis alone. Therefore, hadronic models are needed to describe the specifics of in-medium changes of vector mesons.

The first experimental observations of a significant reshaping of the spectral function of the ρ meson have been made by the NA45 [15, 16, 17, 18] and HELIOS [19] collaborations by a measurement of the dilepton invariant mass spectrum obtained in heavy ion collisions. The dilepton spectra show a considerable enhancement over the standard hadronic cocktail calculations consistent with spectral strength moving downward to smaller invariant masses [20, 21, 22, 23]. More recently the NA60 collaboration has obtained dilepton spectra in heavy-ion collisions with unprecedented mass resolution [24]; these results point to a considerable broadening of the ρ meson, but no mass shift.

The observed signals in heavy-ion collisions necessarily represent time-integrals over very different stages of the collision (from initial non-equilibrium states over equilibrium in the QGP and/or hadronic phase) with significantly changing densities and temperatures. It has, therefore, been stressed [25] that experiments with elementary probes on normal nuclei can yield signals for in-medium changes that are as large as those obtained in heavy-ion collisions. Such experiments using more elementary projectiles like photons, protons and pions are of special interest as they provide an excellent testing ground for theoretical models based on the assumption of nuclear matter in equilibrium with only moderate densities ($\leq \rho_0$) [26, 27] (how to go beyond this low density approximation see [28]). Following this proposal, a recent investigation of the dilepton invariant mass spectrum in pA reactions interpreted in terms of a modification of the ρ and ω spectral densities has been made at KEK [29, 30, 31]. A different approach has been chosen by the CB/TAPS collaboration by investigating the $\pi^0\gamma$ channel in γA reactions, hence focusing exclusively on the properties of the ω meson [32], see also [33, 34]. Another promising experiment that is being analyzed by the CLAS collaboration has taken dielectron data from γA reactions [35], see [36] for a theoretical approach.

In the following we concentrate on the ω-meson. (Concerning theoretical investigations of the ρ-meson we refer to [28, 37] and references therein.) A lot of theoretical effort has already been put into the determination of the isoscalar spectral density in nuclear matter [12, 38, 39, 40, 41, 42, 43, 44, 45, 46, 47, 48, 49]. The outcome of these works covers a rather large area in the mass/width plane, ranging for the mass from the free ω pole

mass (782 MeV) down to roughly 640 MeV and for the width up to about 70 MeV. These approaches differ quite substantially in their methodical background. Some of them find a shift of spectral strength to lower invariant masses [39, 41, 42, 43, 46] whereas others obtain an upwards shift [9, 44, 45, 50, 51]. For a later comparison to our result we will pick out two rather different approaches: In the model of [45] the in-medium self energy of the ω is driven by the collective excitation of resonance-hole loops. The rather large couplings of the $D_{13}(1520)$ and $S_{11}(1535)$ nucleon resonances to the $N\omega$ channel lead to an additional peak in the spectral function, whereas the ω branch itself even moves to slightly higher masses due to level repulsion. The model of [12, 41] is based on an effective Lagrangian which combines chiral SU(3) dynamics and vector meson dominance. No resonances besides the $\Delta(1232)$ are considered. The authors of [12, 41] find a rather drastic downward shift of the ω pole mass with rising baryon density that can be interpreted as an effect of the renormalization of the pion cloud generated by the strong interaction between pions and nucleons.

Both approaches [45] and [12, 41] use the fact that to lowest order in the nuclear density the ω in-medium self energy is proportional to the ωN forward scattering amplitude which is not directly accessible in experiments. One solution to this problem is to use a unitary coupled-channel approach to constrain the ωN amplitude. Such calculations have been performed in [45] where important contributions from nucleon resonance excitations were found. These resonances were created dynamically in [45] starting from a Lagrangian with contact interactions. The latter have to be introduced separately for each partial wave with new input parameters to be fitted to experimental data. Therefore the authors of [45] restrict themselves to angular momentum $L = 0$ between nucleon and vector meson. This imposes a restriction to the energy region close to threshold where no contributions from the partial waves with $L > 0$ must be taken into account. On the other hand, this simplifying approximation that the ω meson is at rest with respect to the surrounding nuclear matter is not a valid assumption for modeling nuclear reactions as the involved momenta of the produced mesons can acquire quite large values, see e.g. [33, 52].

In the present work we eliminate this problem by constructing the ωN scattering amplitude from the unitary coupled-channel K-matrix approach developed in [53, 54, 55, 56, 57, 58]. This approach is based on an effective Lagrangian including resonance fields and aims at a reliable extraction of nucleon resonance properties from experiments where the nucleon is excited via either hadronic or electromagnetic probes. The model simultaneously

describes all available data on pion- and photon-induced reactions on the nucleon for energies $\sqrt{s} \leq 2$ GeV, including the final states γN, πN, $2\pi N$, ηN, ωN, $K\Lambda$ and $K\Sigma$. The same Lagrangian is used for pion- and photon-induced reactions, allowing for the extraction of a consistent set of parameters. In contrast to other approaches the model includes all resonance states with quantum numbers $J^P = \frac{1}{2}^{\pm}, \frac{3}{2}^{\pm}$ and $\frac{5}{2}^{\pm}$ up to masses of 2 GeV and can thus be used to calculate the self energy also for finite ω momenta.

The paper is organized as follows: in Section II A we outline the calculation of the ω in-medium self energy. Section II B gives an overview over the coupled-channel resonance model and its application to the case at hand. In Section III we explore the role of resonance contributions and coupled-channel effects. The results are discussed in Section IV. Finally we summarize our findings in Section V. In the Appendices some technical details of the calculations are given.

II. THE MODEL

A. Vector mesons in nuclear matter

The properties of a vector meson at finite nuclear density are characterized by its spectral function $\mathcal{A}_V$ which is the imaginary part of the retarded in-medium vector meson propagator:

$$\begin{aligned} \mathcal{A}_V^{T/L}(q) = -\frac{1}{\pi}\mathcal{I}m\ D_V^{T/L}(q) &= -\frac{1}{\pi}\mathcal{I}m\ \frac{1}{q^2 - m_V^2 - \Pi_{\rm vac}(q) - \Pi_{\rm med}^{T/L}(q)} \\ &= -\frac{1}{\pi}\frac{\mathcal{I}m\Pi_{\rm tot}^{T/L}(q_0,\mathbf{q})}{\left(q_0^2 - \mathbf{q}^2 - m_V^2 - \mathcal{R}e\Pi_{\rm tot}^{T/L}(q_0,\mathbf{q})\right)^2 + \left(\mathcal{I}m\Pi_{\rm tot}^{T/L}(q_0,\mathbf{q})\right)^2} \end{aligned} \tag{1}$$

with the vector meson four momentum $q = (q_0, \mathbf{q})$. In the following we are only concerned with the in-medium self energy $\Pi_{\rm med}$ and will therefore drop the index $\Pi_{\rm med} = \Pi$. The vacuum self energy $\Pi_{\rm vac}$ entering the ω spectral function will be discussed briefly in Appendix A.

The self energies $\Pi^{T/L}(q)$ depend independently on both variables q_0 and $|\mathbf{q}|$. The indices ^{T} and ^{L} denote the projections on the transverse and longitudinal modes of the vector meson which are obtained by contracting the self energy with the three-transverse and the three-longitudinal projectors:

$$\Pi^T = \frac{1}{2}P_T^{\mu\nu}\Pi_{\mu\nu}\,,$$

$$\Pi^L \;=\; P_L^{\mu\nu}\Pi_{\mu\nu}. \tag{2}$$

For a definition of $P_T^{\mu\nu}$ and $P_L^{\mu\nu}$ see e.g. [28].

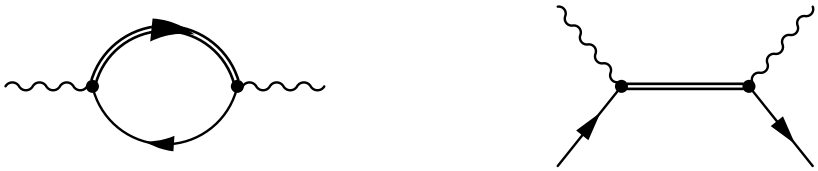

(a) (b)

FIG. 1: Lowest order contribution to the vector meson self energy in nuclear matter (a) and vector meson nucleon scattering via excitation and decay of an s-channel resonance (b).

In the present work we use the low-density theorem [59] to determine the in-medium self energy of the ω-meson. We start by illustrating this theorem by a specific (and important) type of process: From the coupling of the vector meson to baryon resonances, the contribution to the in-medium self energy $\Pi_{\mu\nu}$ is given to lowest order by the diagram depicted in Fig. 1(a). Applying standard Feynman rules, considering for illustration a resonance R with spin $\frac{1}{2}$ and neglecting the u-channel contribution, one arrives at the following expression [60]:

$$i\Pi_{\mu\nu}(q) = (-ig)^2(-1)\int \frac{d^4p}{(2\pi)^4}\mathrm{Tr}\left\{\Gamma_\mu G_N(p)\Gamma_\nu G_R(k)\right\}, \tag{3}$$

where we have assumed a not further specified coupling at the RNV vertex of the form

$$\mathcal{L}_{RNV} \sim g\bar{u}_R\Gamma_\mu u_N V^\mu. \tag{4}$$

The momentum of the resonance is $k = p + q$. G_N and G_R denote the (in-medium) propagators of the nucleon and the spin-$\frac{1}{2}$ resonance. By inserting the relativistic in-medium nucleon propagator into Eq. (3) and keeping only the relevant part corresponding to the propagation of nucleon holes, the above expression simplifies to

$$\Pi_{\mu\nu}(q_0,\mathbf{q}) = g^2\int \frac{d^3p}{(2\pi)^3}\frac{1}{2E_N(\mathbf{p})}\Theta(p_F-|\mathbf{p}|)\mathrm{Tr}\left\{\Gamma_\mu(\not{p}+m_N)\Gamma_\nu G_R(k)\right\}, \tag{5}$$

where we have introduced the nucleon Fermi momentum in the local density approximation

$$p_F = \left(\frac{3}{2}\pi^2\rho\right)^{\frac{1}{3}}\;; \tag{6}$$

ρ denotes the nucleon density. The trace Tr$\{\ldots\}$ in Eq. (5) is proportional to the forward scattering tensor $T_{\mu\nu}$ for the process $V(q)N(p) \to R(k = p + q) \to V(q)N(p)$, depicted in Fig. 1(b). In the limit of low densities, the **p**-dependence of the scattering tensor can be neglected, allowing to carry out the integral explicitly. Hence we arrive at the simple expression:

$$\Pi_{\mu\nu} = \rho T_{\mu\nu}, \tag{7}$$

which is known as the low density theorem [59]. Eq. (7) is a very general expression which is not restricted to the formation of resonances. It holds basically for all processes involving one nucleon line at a given time. To get the complete self energy one needs the complete ω-nucleon forward scattering amplitude in (7). In the following section we show how the not directly measurable ωN forward scattering tensor can be obtained by solving the coupled-channel scattering problem.

B. The ω-nucleon scattering amplitude

An extensive description of the coupled-channel approach has been given in [55, 56, 57, 58, 61] and references therein. Here we briefly outline some of the main features of the model focusing mainly on the ωN scattering tensor.

The $2 \to 2$ scattering amplitude is obtained by summing the two-body interaction potential to all orders, while the physical constraints as relativistic invariance, unitarity and gauge invariance are preserved. This corresponds to a solution of the Bethe-Salpeter equation that is shown graphically in Fig. 2. Formally, i.e. dropping the arguments and the integration/summation over the intermediate states, the Bethe-Salpeter equation can be written as

$$M = V + V G_{\mathrm{BS}} M \tag{8}$$

with the two-body interaction potential V and the Bethe-Salpeter propagator G_{BS} that is the product of the intermediate state nucleon and meson propagators. M is the full two-body scattering amplitude containing also rescattering effects. To solve this equation the so-called K-matrix approximation is applied. Here the real part of the propagator G_{BS} is neglected, which corresponds to putting all intermediate particles on their mass shell. The

asymptotic particle states considered in our approach are γN, πN, $2\pi N$, ηN, ωN, $K\Lambda$ and $K\Sigma$.

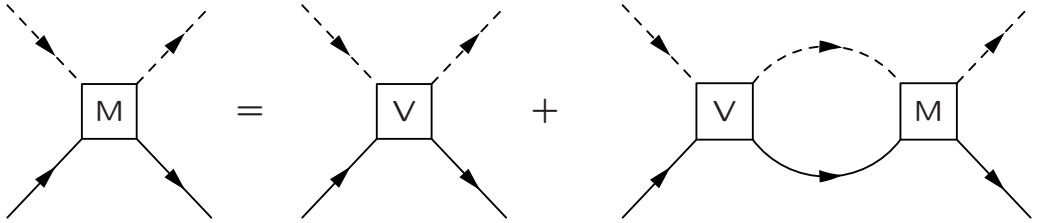

FIG. 2: Bethe-Salpeter equation for the two-particle scattering amplitude.

The interaction potential V entering the Bethe-Salpeter equation is built up as a sum of the s-, u- and t-channel contributions corresponding to the tree-level diagrams shown in Fig. 3. The internal lines in the diagrams (a) and (b) represent either a nucleon or a baryon resonance. In the t-channel exchange diagram (c) the contributions from scalar, pseudoscalar and vector mesons are taken into account, see e.g. [58]. Thus, resonance and background contributions are generated consistently from the same interaction Lagrangians. The Lagrangians used to construct the K-matrix kernel are given in the literature [55, 56, 57, 58]. For completeness, the resonance $RN\omega$ couplings are summarized in Appendix B. Applying a partial wave decomposition of the scattering amplitudes, Eq. (8) can be rewritten in the K-matrix approximation in the form

$$T_{ij}^{J^{\pm},I} = K_{ij}^{J^{\pm},I} + i \sum_{k} T_{ik}^{J^{\pm},I} K_{kj}^{J^{\pm},I}, \tag{9}$$

where $T_{ij}^{J^P,I}$ is a scattering amplitude for the total spin J, parity P and isospin I. The indices i, j, k denote the various final states $i, j, k = \pi N$, $2\pi N$, ωN, etc.

In such a treatment of the scattering problem the transition amplitudes $T_{\omega N \to \omega N}^{J^{\pm}}$ are the result of solving the coupled-channel equation (9) where resonance contributions and rescattering effects are included in a selfconsistent way. In a previous calculation [58] the updated solution to the $\pi N \to \gamma N$, πN, $2\pi N$, ηN, ωN, $K\Lambda$, $K\Sigma$ and $\gamma N \to \gamma N$, πN, ηN, ωN, $K\Lambda$, $K\Sigma$ reactions in the energy region $\sqrt{s} \leq 2\,\mathrm{GeV}$ has been obtained. The a priori unknown resonance coupling constants have been obtained from the fit to all available experimental reaction data in the energy region under discussion. As a result of these calculations the elastic ωN scattering amplitudes of interest have been extracted. Here,

we use these amplitudes as an input for the calculation of the ω spectral function at finite nuclear density by means of the low-density theorem.

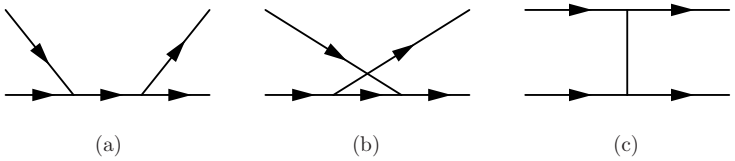

FIG. 3: s-, u- and t-channel contributions to the interaction kernel.

For the case at hand we have extended our coupled-channel model in order to allow for arbitrary four momenta of the ω meson as required by Eq. (1). Thus, we are interested in the forward scattering amplitude as a function of the two independent variables $|\mathbf{q}|$ and q_0 or, alternatively, q^2. The extension is achieved by introducing an additional final state into the Bethe Salpeter equation (9) that we call $N\omega^*$. Such an additional 'effective' ω^* meson is characterized by completely identical properties as the physical ω meson apart from its mass $\sqrt{q^2}$ that can take arbitrary values. To calculate the amplitude $T_{\omega^* N}$ as a function of $q^2_{\omega^*} = m^2_{\omega^*} \neq m^2_\omega$ we follow the procedure used in [56] to describe photon-induced reactions on the nucleon. With the amplitudes from Eq. (9) we obtain

$$T^{J^\pm,I}_{\omega^* N,i} = K^{J^\pm,I}_{\omega^* N,i} + i \sum_{j \neq \omega^* N} K^{J^\pm,I}_{\omega^* N,j} T^{J^\pm,I}_{j,i}, \tag{10}$$

$$T^{J^\pm,I}_{\omega^* N,\omega^* N} = K^{J^\pm,I}_{\omega^* N,\omega^* N} + i \sum_{j \neq \omega^* N} K^{J^\pm,I}_{\omega^* N,j} T^{J^\pm,I}_{j,\omega^* N}, \tag{11}$$

where the amplitudes $T^{J^\pm,I}_{j,i}$ are solutions of the coupled-channel problem taken from [58]. The matrices $K^{J^\pm,I}_{\omega^* N,i}$ contain the interaction potential for the transitions $\omega^* N \to \omega^* N$, ωN, πN, etc., and are chosen to be the same as $K^{J^\pm,I}_{\omega^N,i}$ but with $m_{\omega^*} \neq m_\omega$. It is easy to see that for $q^2_{\omega^*} = m^2_{\omega^*} = m^2_\omega$ the amplitudes $T_{\omega^* N}$ from Eq. (11) and $T_{\omega N}$ in Eq. (9) become equal. Note, that introducing the $\omega^* N$ final state does not destroy the unitarity of $T_{\omega N}$ since the $\omega^* N$ channel does not appear in the intermediate state in Eq. (11). In this way we obtain the vacuum scattering amplitude entering the low density theorem: The in-medium ω meson (the outer legs) can take arbitrary four momenta $(q_0, \mathbf{q})$, whereas the internal lines maintain the vacuum properties of the ω and all other mesons, i. e. the four momentum of the internal ω is constrained by the on-shell condition $q_0 = E_\omega(\mathbf{q}) = \sqrt{m^2_\omega + \mathbf{q}^2}$. This corresponds to a

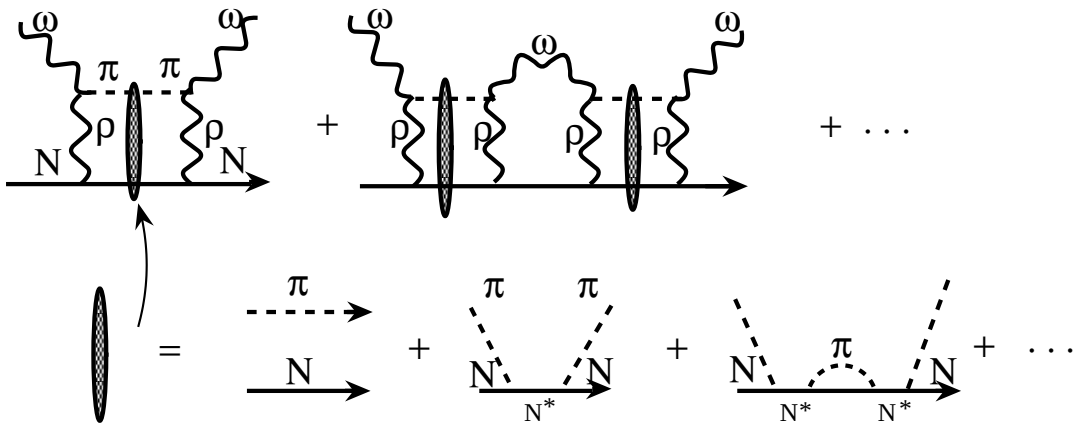

FIG. 4: Simplified model for ωN scattering to explore the effect of resonance excitations. $T_{\omega N}$ is a sum of an infinite series of diagrams (upper panel) with the $S_{11}(1650)$ resonance excitation in the intermediate πN channel.

first order expression in the nuclear density, taking into account only interactions with one nucleon at a time.

III. THE ROLE OF RESONANCE CONTRIBUTIONS

The ωN scattering amplitude derived in [58] and used in the present calculations is a coherent sum of resonance and background contributions including multi-rescattering effects in a number of intermediate channels: πN, $2\pi N$, etc. In contrast, the work of [12, 41] uses only Born and mesonic box diagrams with the Δ being the only resonance excitation considered. In this Section we, therefore, illustrate the importance of a single resonance excitation at ~ 1.65 GeV and coupled-channel effects. To this end we construct a simplified model for ωN scattering where the transition amplitude under discussion is a sum of the infinite series of diagrams shown in Fig. 4. It corresponds to solving the coupled-channel Bethe-Salpeter equation in the K-matrix approximation with the ωN and πN channels including also the transitions $\pi N \to \omega N$. As a showcase we take into account the excitation of the $S_{11}(1650)$ resonance in the intermediate πN channel. The choice of this resonance is motivated by its mass which is close to the ωN threshold. Note that here this resonance contributes to ωN scattering only indirectly via the rescattering in the intermediate πN channel.

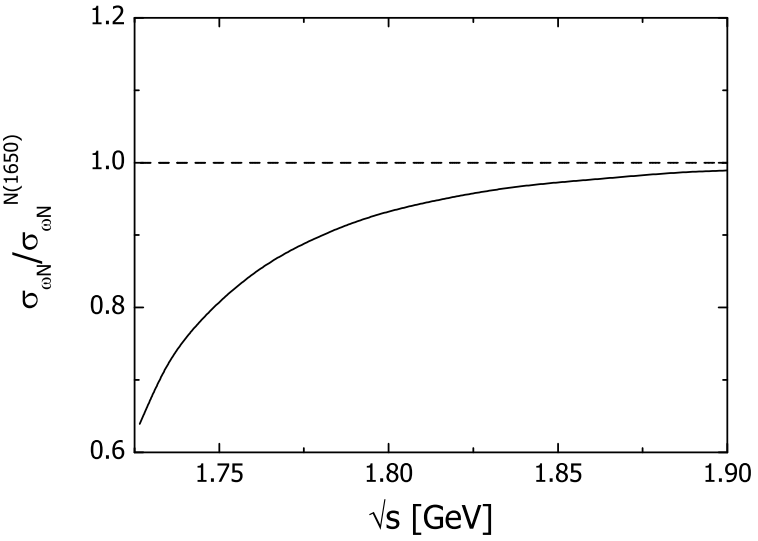

FIG. 5: Ratio of total cross section calculated within the simplified model displayed in Fig. 4 without resonance contributions ($\sigma_{\omega N}$) to that including the $S_{11}(1650)$ state ($\sigma_{\omega N}^{N(1650)}$).

To explore the role of the $S_{11}(1650)$ resonance excitation we calculate the total cross sections $\sigma_{\omega N}$ using $\Gamma^{\pi N}_{N(1650)} = 0$ and $\sigma_{\omega N}^{N(1650)}$ using $\Gamma^{\pi N}_{N(1650)} = 95$ MeV, respectively. Thus, in the first case the resonance contributions are absent. The non-resonance couplings are chosen in accordance with [58]. Form factors are neglected for the sake of simplicity. To minimize the dependence on the choice of the coupling constants at the non-resonance vertices we calculate the ratio of the total cross sections $\sigma_{\omega N}/\sigma_{\omega N}^{N(1650)}$ that is shown in Fig. 5 as a function of the c.m. energy. One can see a dramatic change of the ωN scattering once the contribution from the $S_{11}(1650)$ resonance is included. As was expected the main difference between the two calculations is found in the energy region close to the resonance pole. At higher energies the contribution from the $S_{11}(1650)$ vanishes and both results coincide. Note, that no direct resonance couplings to the ωN channel are allowed in these calculations. We conclude that for a realistic description of the ωN scattering amplitude coupled-channel effects must be taken into account. The contributions from nucleon resonances cannot be neglected even for vanishing resonance couplings to the ωN final state.

IV. RESULTS

According to the low-density theorem, the ω spectral function is entirely determined by the forward scattering amplitude $T_{\omega N}$. At zero momentum the latter reduces to the scattering length. Hence, the ωN scattering length $a_{\omega N}$ defines the ω meson self energy at the physical mass. In [58] the scattering lengths and effective radius have been extracted from the ωN scattering amplitude. Here, we follow [41] and define $a_{\omega N}$ in a slightly different way which is useful for the present calculations (see Appendix C). For the ωN scattering length we obtain the values

$$\begin{aligned} a_{\omega N} &= a_{\omega N}^{\frac{1}{2}^-} + a_{\omega N}^{\frac{3}{2}^-} = (-0.17 + i0.31)\ \text{fm}, \\ a_{\omega N}^{\frac{1}{2}^-} &= (-0.27 + i0.16)\ \text{fm}, \\ a_{\omega N}^{\frac{3}{2}^-} &= (+0.11 + i0.15)\ \text{fm}, \end{aligned} \tag{12}$$

where $a_{\omega N}^{\frac{1}{2}^-}$ and $a_{\omega N}^{\frac{3}{2}^-}$ are the contributions from the spin $\frac{1}{2}$ (S_{11}) and spin $\frac{3}{2}$ (D_{13}) sector, respectively. While we find an attraction in the D_{13} wave the contribution from S_{11} dominates the real part leading to the slight overall repulsion in the ωN system. This result has to be compared with $a_{\omega N} = (1.6 + i0.3)$ fm obtained by Klingl et el. [41] and $a_{\omega N} = (-0.44 + i0.2)$ fm obtained by Lutz et al. [45]. While the imaginary parts in all three calculations are similar, there is a spread of values in the real part; we will comment later on this variation.

In Fig. 6 the ω spectral function at finite nuclear densities $\rho = 0,\ \rho = \rho_0 = 0.16\ \text{fm}^{-3}$ and $\rho = 2\rho_0$ is shown for an ω meson that is at rest with respect to the surrounding nuclear matter. The appropriately normalized data points correspond to the process $e^+e^- \to \gamma^* \to \omega \to \pi^+\pi^-\pi^0$ that directly resembles the ω vacuum spectral function. Most noticeable the ω meson survives as a quasi particle at nuclear saturation density which is in agreement with all competing approaches known by the authors. The main effect of the in-medium self energy is a considerable broadening of the peak that amounts to roughly 60 MeV at $\rho = \rho_0$. This value is in line with a recent attenuation analysis [64]. The peak position is shifted upwards only slightly by about 10 MeV. Due to the collective excitation of resonance hole loops the spectral function shows a second peak at low values of the ω invariant mass $\sqrt{q^2}$.

The ω in-medium self energy including the excitation of resonance-hole pairs exhibits a remarkably rich structure, see Fig. 7, where we show the real and imaginary part of the ω self energy of both the longitudinal and transverse mode for three-momenta $|\mathbf{q}| =$

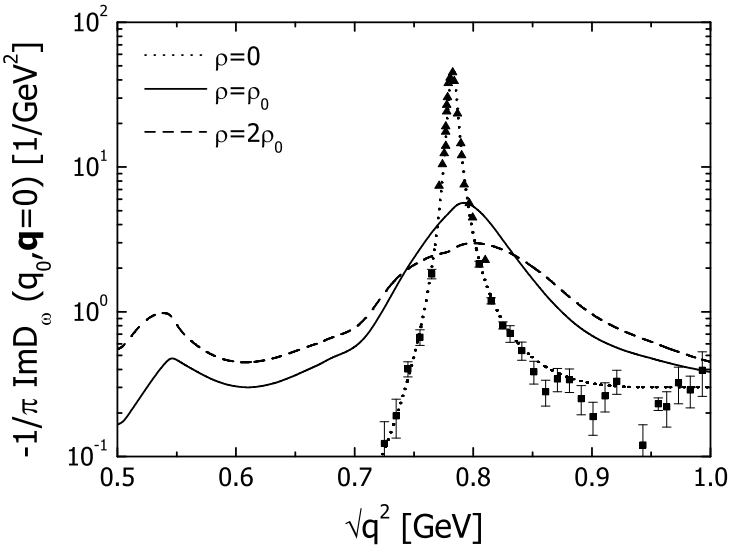

FIG. 6: The ω spectral function for an ω meson at rest, i.e. $q_0 = \sqrt{q^2}$. The appropriately normalized data points correspond to the reaction $e^+e^- \to \omega \to 3\pi$ in vacuum, taken from Ref. [62, 63]. Shown are results for densities $\rho = 0$, $\rho = \rho_0 = 0.16$ fm^{-3} (solid) and $\rho = 2\rho_0$ (dashed).

0 MeV, 300 MeV and 600 MeV at normal nuclear matter density. In the limit of very small resonance widths, each resonance-hole pair generates an additional branch in the spectral distribution which leads to a multi peak structure. As the widths of most of the involved resonances for the case at hand are large, see Table I, almost no individual peaks can be distinguished and the resonance excitations add up to a background like structure.

However, for the ω meson at rest one additional peak in both the imaginary part of the self energy and the spectral function can be identified at ~ 0.55 GeV (see Figs. 7 and 6). This branch of the ω spectral function is due to the excitation of the $S_{11}(1535)$ resonance. This resonance couples in relative s-wave to the $N\omega$ channel and dominates the spectrum at low ω momenta and low q^2. Note, that the authors of [45] come to the same conclusion on the role of the $S_{11}(1535)$ state. However, contrary to [45] we see no prominent effect from $D_{13}(1520)$ because of the smaller coupling of this resonance to the ωN final state. The invariant mass $\sqrt{q^2}$ of the $S_{11}(1535)$ resonance-hole branch moves to smaller values as the three-momentum increases and can approximately be determined by the kinematical relation

$$(q+p)^2 = q^2 + m_N^2 + 2m_N\sqrt{q^2+\mathbf{q}^2} = m_R^2. \tag{13}$$

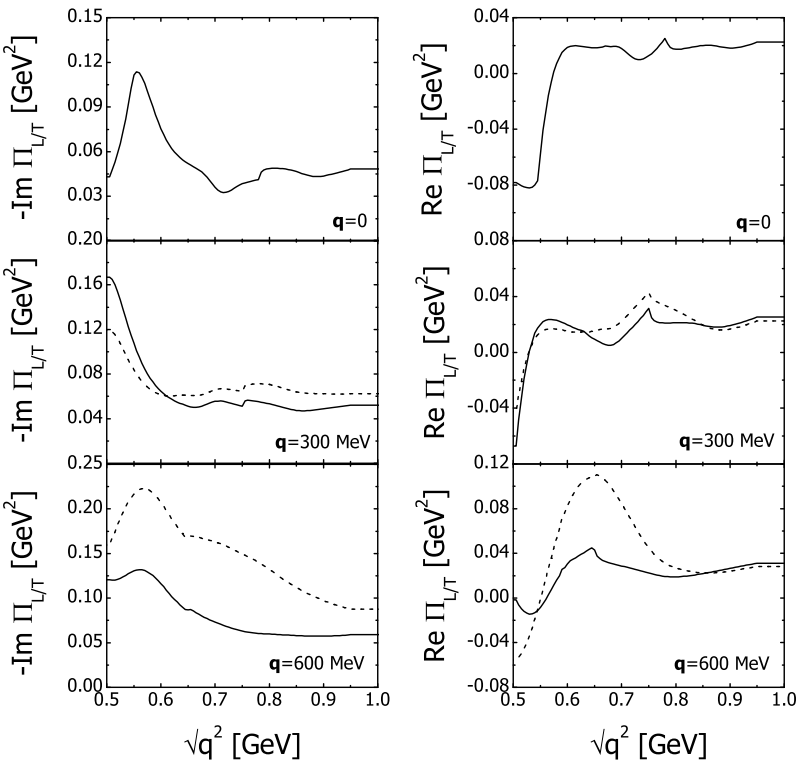

FIG. 7: Real (right panel) and imaginary (left panel) part of the ω self energy in nuclear matter at saturation density $\rho_0 = 0.16$ fm^{-3}. Shown are the longitudinal (solid) and transverse (dashed) modes for ω three-momenta $|\mathbf{q}| = 0$, $|\mathbf{q}| = 300$ MeV, $|\mathbf{q}| = 600$ MeV with respect to nuclear matter at rest.

Therefore, in Fig. 7 the resonance-hole peak visible at a mass of $\sqrt{q^2} \approx 550$ MeV for zero momentum moves down to $\sqrt{q^2} \approx 500$ MeV for a momentum of 300 MeV.

Another interesting structure is visible in Fig. 7 at masses of 782 MeV ($|\mathbf{q}| = 0$ MeV), 750 MeV ($|\mathbf{q}| = 300$ MeV) and 649 MeV ($|\mathbf{q}| = 600$ MeV). This cusp structure is due to the opening of the elastic channel $\omega^*(\sqrt{q^2})N \to \omega(782)N$, i.e. the scattering of the off-shell ω^* into the on-shell ω becomes energetically possible. The position of this threshold is determined by the equation

$$q^2 = m_N^2 + (m_N + m_\omega)^2 - 2m_N\sqrt{(m_N + m_\omega)^2 + \mathbf{q}^2}. \tag{14}$$

We should note that this threshold effect is an artifact of the applied low-density approximation. If the self energy was obtained in an iterative scheme, i. e. taking into account higher order density effects, this cusp structure would be smeared out.

$L_{2I,2S}$	status	mass	$\Gamma_{\rm tot}$	$R_{\pi N}$	$R_{2\pi N}$	$R_{\eta N}$	$R_{\omega N}$	$g^1_{RN\omega}$	$g^2_{RN\omega}$	$g^3_{RN\omega}$
$S_{11}(1535)$	****	1526	136	34.4	9.5	56.1	–	3.79	6.50	–
$S_{11}(1650)$	****	1664	131	72.4	23.1	1.4	–	−1.13	−3.27	–
$P_{11}(1440)$	****	1517	608	56.0	44.0	2.82	–	1.53	−4.35	–
$P_{11}(1710)$	***	1723	408	1.7	49.8	43.0	0.2	−1.05	10.5	–
$P_{13}(1720)$	****	1700	152	17.1	78.7	0.2	–	−6.82	−5.84	−8.63
$P_{13}(1900)$	**	1998	404	22.2	59.4	2.5	14.9	5.8	14.8	−9.9
$D_{13}(1520)$	****	1505	100	56.6	43.4	0.012	–	3.35	4.80	−9.99
$D_{13}(1950)^a$	**	1934	859	10.5	68.7	0.5	20.1	−10.5	−0.6	17.4
$D_{15}(1675)$	****	1666	148	41.1	58.5	0.3	–	109	−99.00	83.5
$F_{15}(1680)$	****	1676	115	68.3	31.6	0.0	–	12.40	−35.99	−78.28
$F_{15}(2000)$	**	1946	198	9.9	87.2	2.0	0.4	−19.6	19.3	23.14

TABLE I: Properties of the $J^P = \frac{1}{2}^\pm, \frac{3}{2}^\pm$ and $\frac{5}{2}^\pm$ resonances that couple to the $N\omega$ channel. Masses and widths are given in MeV and the on-shell decay ratios R are given in percent. The current status is quoted as in Ref. [65]. In addition, also the $RN\omega$ coupling constants entering the Lagrangians (Appendix B) are given. ^{a}: in Ref. [65] listed as $D_{13}(2080)$.

In Fig. 8 we show the longitudinal and transverse mode of the ω spectral function for momenta of $|\mathbf{q}| = 0$ MeV, 300 MeV and 600 MeV.

We observe a significantly different momentum dependence of the two helicity states: $\mathcal{A}^T$ is strongly affected at large ω momenta whereas $\mathcal{A}^L$ remains almost unchanged. We note in passing that this resembles qualitatively the spectral functions for the in-medium ρ-meson calculated in [28].

The same effect is visible in the calculation of the ω width evaluated at the actual peak position of the ω branch. It is given by the expression

$$\Gamma^{L/T}_{\rm peak}(\mathbf{q}) = -\frac{\mathcal{I}m\Pi^{L/T}\left(q_0 = (m^2_{\rm peak} + \mathbf{q}^2)^{\frac{1}{2}}, \mathbf{q}\right)}{m_{\rm peak}}. \tag{15}$$

In Fig. 9 we show $\Gamma^L_{\rm peak}(\mathbf{q})$ and $\Gamma^T_{\rm peak}(\mathbf{q})$ as a function of the ω three-momentum. For an ω meson at rest the collisional broadening amounts to roughly 60 MeV at normal nu-

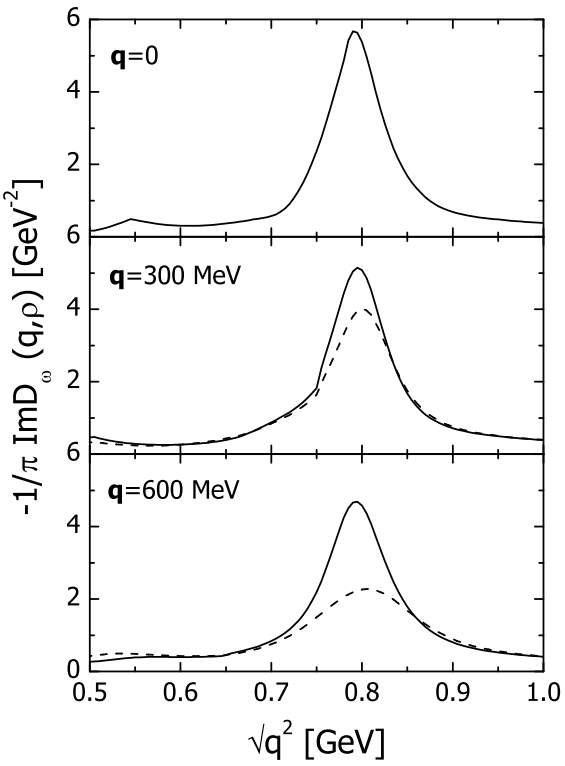

FIG. 8: The transverse (dashed) and longitudinal (solid) modes of the ω spectral function at nuclear saturation density $\rho_0 = 0.16$ fm^{-3}. Shown are results for ω three-momenta $|\mathbf{q}| = 0$, $|\mathbf{q}| = 300$ MeV, $|\mathbf{q}| = 600$ MeV with respect to nuclear matter at rest.

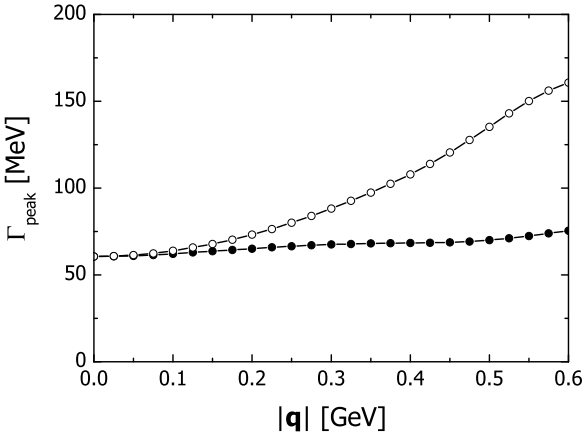

FIG. 9: The ω width in nuclear matter at the actual peak position of the spectral function for different laboratory momenta. Open symbols correspond to transversely and solid symbols to longitudinally polarized ω mesons.

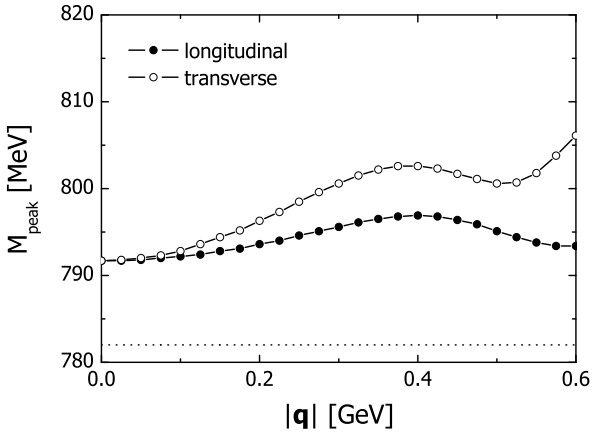

FIG. 10: Peak position of the ω spectral distribution in matter at ρ_0. Open symbols correspond to the transverse and solid symbols to the longitudinal modes. The dotted line denotes the value of the free ω peak mass.

clear matter density. For finite three-momentum this width more or less stays constant for the longitudinal branch whereas it drastically rises for the transverse modes. From Eqs. (7,15) it follows that the widths of the longitudinal and transverse modes, $\Gamma_{\rm peak}^{L/T}(\mathbf{q})$, are entirely defined by the imaginary parts of the ωN scattering amplitudes $\mathcal{I}m\left\{T_{0+\frac{1}{2}}\right\}$ and $\frac{1}{2}\mathcal{I}m\left\{T_{1-\frac{1}{2}}+T_{1+\frac{1}{2}}\right\}$, correspondingly (see Appendix C). The lower subscript denotes the helicities of the ω-meson and the nucleon. Note, that at the ωN threshold only the $J=\frac{1}{2}^-$ and $J=\frac{3}{2}^-$ partial waves contribute. Since the ωN scattering is dominated by the resonance mechanism the helicity amplitudes are governed by the $RN\omega$ coupling constants extracted in [58]. They are given in Table I for completeness. The different $RN\omega$ coupling constants correspond to various helicity combinations of the ωN final state, see [55, 58] for details. With increasing ω momentum the resonance contributions become more important giving main contributions to the $(1,-\frac{1}{2})$ and $(1,+\frac{1}{2})$ helicity amplitudes. As a result the transverse mode is strongly modified with increasing ω momentum.

The peak position of the genuine ω branch in both spectral functions moves only slightly to higher q^2 values as can be seen also in Fig. 10. This is due to level repulsion as the most important resonance-hole states are subthreshold with respect to the $N\omega$ channel. Since the scattering amplitude $T_{\omega N}$ used in our calculations is a coherent sum of a number of resonance contributions including coupled-channel effects the separation of individual resonance contributions is difficult. However, several conclusion can be drawn. First, over

the full energy range under consideration the self energy is dominated by resonance hole excitations, whereas the nucleon Born terms give only marginal contributions. Although the excitation of resonance-hole states leads to additional branches in the spectral functions, no clearly distinguishable peak structures emerge due to the large widths and the only moderate coupling to the $N\omega$ channel of the individual resonances. This is also suggested by pion- and photon-induced ω production data which do not show any prominent resonance structures. The ωN amplitude at threshold is dominated by the $S_{11}(1535)$ resonance and – through background (u-channel) contributions – by the $D_{15}(1675)$ and $F_{15}(1680)$ states. At zero momentum the $S_{11}(1535)$ resonance generates strength at low invariant masses. The u-channel contributions of the $P_{11}(1710)$ and $F_{15}(1680)$ resonances that lie only slightly subthreshold to the $N\omega$ channel due to level repulsion push the ω branch to higher q^2 values.

We now compare our results to those obtained from other models. Very close in spirit to our approach is the work of [45] that is also based on a solution of a coupled-channel Bethe Salpeter equation. This analysis is restricted to ω mesons at rest as no p-wave resonances have been incorporated. At least qualitatively the results of [45] compare very well to our findings: Due to resonance-hole excitations an additional peak in the spectral function was found (however much stronger and stemming from the unresolved contributions of the $D_{13}(1520)$ and $S_{11}(1535)$ resonances) whereas the genuine ω peak is shifted only slightly upwards in energy.

In [12, 41] the main contribution to the ω medium modification comes from a change of the $\rho\pi$ self energy generated by the ρN and πN interactions. Whereas the on-shell broadening obtained by the authors of Ref. [41] compares very well to our value of roughly 56 MeV, they find an extremely strong attractive mass shift that is not found in our calculations. In [12, 41] the real part of the in-medium self energy, that determines the peak position of the spectral function, is obtained by a dispersion relation. The magnitude and in particular the energy dependence of this real part can be attributed to the strong energy variation of the $\omega N \to 2\pi N$ cross section which in [41] is dominated by the scattering into an intermediate ρN state. We note that this $2\pi N$ final state is not constrained by any data in the calculations of [41]. In contrast, in our approach the $2\pi N$ final state is constrained by the coupled-channel mechanism. In particular, it has to account for the inelasticity in the pion-induced reaction channels. This results in a more moderate energy dependence of the corresponding cross sections and, hence, — via dispersion — in a smaller real part of the scattering amplitude.

We also stress, that the self energy in [41] is obtained from a pure tree level calculation using the heavy-baryon approximation whose reliability is questionable for the nucleon lines. Furthermore, we have illustrated in Sect. III that the coupling of the ωN and πN channels to nucleon resonances yields important contributions to the ω in-medium spectrum that are absent in the calculation of [41]. In spite of the fact that in our approach the $2\pi N$ final state is constrained by inelasticity data, one should note that this $2\pi N$ channel as a three-body state is not treated as rigorously as the two-body states (πN, ηN, $K\Lambda$, ...). This is due to the fact that the inclusion of a three-particle state in a K-matrix approach is much more complicated. Clearly this leaves some room for further theoretical improvements.

Recent experiments by the CBELSA/TAPS collaboration [32] have found an in-medium width of the ω meson extrapolated to small three-momenta of the ω of about 50 MeV. This result for the width is in agreement with the calculations presented here (Fig. 9). In [32] also a mass shift down to a peak mass of about 720 MeV has been observed. This value has been obtained for the integrated ω momentum spectrum from 0 to 500 MeV in this photoproduction experiment carried out at beam energies from 0.64 GeV to 2.53 GeV. The latter result is not in agreement with our calculations. This raises the immediate question for an interpretation of the experimentally observed effect and its relation to the calculations presented here.

We first note that the observed mass spectrum cannot directly be compared to the spectral function calculated in this paper since the experimental results represent a product of the spectral function with the branching ratio into the $\pi^0\gamma$ channel. The dominant $\rho\pi$ decay branch increases with mass whereas that for the $\pi^0\gamma$ decay is much flatter as a function of the ω mass (see Fig. 6 in [64]). Multiplying the spectral function with the relevant branching ratio thus tends to shift strength down towards smaller masses. This effect has not been taken into account in the analysis of the CBELSA/TAPS experiment. Moreover, the branching ratio is expected to change in the medium along with the ρ meson properties. We also note that the effect observed experimentally obviously depends on the background subtraction.

In principle, a similar effect could also be generated by low-lying resonance-hole excitations that leave the position of the generic ω peak almost untouched. Our calculations presented here contain prominent resonance-hole components only at much lower energy (see Fig. 6) associated with the $N^*(1535)$ nucleon resonance. The absence of higher-lying

resonance excitations is due to the fact that the most recent K-matrix coupled channel analysis on which the present calculations are based [58] ascribes most of the cross section in γN and πN reactions at threshold to a combination of various background terms and small resonance contributions. On the contrary, the earlier analysis by Penner et al. [55, 56], based on older data and not taking into account the spin-5/2 resonances, gave a much more dominant contribution of the $P_{11}(1710)$ resonance. Building a resonance-hole excitation with this state would indeed give a low-mass component at an energy close to the peak energy of the ω. This illustrates the difficulties that arise in predictions of the ω self energy in medium due to the still evolving experimental situation as far as the ω coupling to nucleon resonances is concerned. As a consequence, theoretically the real part of the ω self energy still is associated with large error bars due to the inelastic ωN channels that are hardly constrained experimentally.

As already indicated in the introduction a discussion of our results in the context of in-medium QCD sum rules seems to be expedient. In [51] a sum rule analysis of the ω in-medium spectrum has been done. With this aim a new type of sum rule – the so-called *weighted finite energy sum rule* – for the study of in-medium vector mesons has been established. It has the advantage to exclusively relate in-medium hadronic and partonic information instead of mixing in-medium and vacuum properties. Moreover, one is essentially free of the problem how to determine a reliable Borel window – an arbitrary mass scale that has to be introduced in order to improve the convergence of the involved dispersion integrals. The authors of [51] have shown that the sum rules cannot readily determine the in-medium spectral shape of the ω meson. For a given hadronic model of the ω spectral function rather some hadronic parameters can be constrained or correlated. Using typical hadronic parametrizations for the ω in medium spectral function a general tendency towards an upwards shift of the ω mass in the medium has been found. This statement, however, strongly depends on the in-medium four-quark condensate, a quantity whose density-dependence is far from settled as yet, see also Refs. [10, 11, 51] for a discussion of this issue.

A sum rule check of the results presented here is, however, delicate. In the sum rules the hadronic information is encoded in the current-current correlation function. Usually the correlator in the vector-isoscalar channel is related to the ω meson using strict vector meson dominance (VMD) what means that the interaction of the electromagnetic current in this channel with hadrons is saturated by the ω meson. This strict version of VMD is, however,

excluded by the sum rules as was shown also in [51]. Any other version of VMD needs more microscopic input (see for instance [66]) that is not provided within the K-matrix approach and, thus, is beyond the scope of the present work. At least qualitatively we state that the recent sum rule analysis [51] agrees with the results presented here whereas hadronic models that find a strong downward shift of the in-medium ω mass require a rather extreme scenario of in-medium changes of the four-quark condensates that can hardly be motivated from our present knowledge.

V. SUMMARY

Using the low density theorem we have calculated the ω meson spectral function at finite nuclear density and zero temperature. The ωN forward scattering amplitude is constructed within a unitary coupled-channel effective Lagrangian model previously applied to the analysis of pion- and photon-induced reactions on the nucleon. The resulting amplitude is taken from the updated solution of the coupled-channel problem in the energy region $\sqrt{s} \leq 2$ GeV. To obtain the spectral function of the ω meson we have extended our approach to allow for arbitrary masses and three-momenta of the asymptotic ω meson while the intermediate ω and all other mesons maintain their vacuum properties. This is in line with the low density approximation.

As a general outcome of our investigations we find that coupled-channel effects and resonance contributions play an important role and cannot be neglected when one aims at a reliable extraction of the ω in-medium properties. At normal nuclear density and zero ω momentum we find a significant broadening of about 60 MeV of the ω spectral function but only a small upwards shift of the ω peak relative to the physical ω mass.

Furthermore, our calculations show that at non-zero momentum the transverse part of the spectral distribution is affected by the $(1, +\frac{1}{2})$ and $(1, -\frac{1}{2})$ helicity contributions from the ωN channel coming from the resonance part of the scattering amplitude. This leads to a larger broadening of the transverse mode of the spectral distribution as compared to the longitudinal one. The question of an in-medium mass shift of the ω meson remains to some extent an open issue due to the $2\pi N$ state. In [41] it has been found to be responsible for a strong attractive mass shift. Unfortunately up to the present three-body states cannot be treated in a rigorous way in the K-matrix approach. Nonetheless we would like to stress

again that also such exotic reactions as $\omega N \to 2\pi N$ should be constrained by data as much as possible - if it turns out that such a channel is important for in-medium modifications. The inclusion of this three-body final state into coupled-channel K-matrix calculations is a highly non-trivial task that will be subject to future investigations.

This work has been supported by DFG and BMBF. We thank M. Lutz and W. Weise for discussions on the subject.

APPENDIX A: THE ω MESON IN VACUUM

channel	ratio [%]	width [MeV]
$\pi^+\pi^-\pi^0$	89.6	7.56
$\pi^0\gamma$	8.7	0.73
$\pi\pi$	1.7	0.14

TABLE II: Decay channels, branching ratios and partial widths of the ω meson in vacuum [65]. The value for the $\omega \to 3\pi$ width is chosen somewhat larger as in [65] (but still within the error bars) in order to saturate the total width by the three dominating decay channels.

The hadronic ω vacuum self energy is given as a sum of the contributions coming from the coupling of the ω to the channels 3π, $\pi^0\gamma$ and 2π, adding up to give a total vacuum decay width of about 8.44 MeV. The partial widths are given in Table II. We assume that the $\omega \to 3\pi$ decay proceeds via an intermediate ρ meson, i.e. $\omega \to \rho\pi \to 3\pi$. For the corresponding decay width we find

$$\Gamma_{\omega\to 3\pi}(q^2) = \int_{4m_\pi^2}^{(\sqrt{q^2}-m_\pi)^2} ds \Gamma_{\omega\to\rho\pi}(q^2,s)\mathcal{A}_\rho(s)\frac{\Gamma_{\rho\to\pi\pi}(s)}{\Gamma_\rho^{\rm tot}(s)} \tag{A1}$$

with the ρ vacuum spectral function $\mathcal{A}_\rho$. From the Lagrangians used in our model [61] we obtain

$$\Gamma_{\omega\to\rho\pi}(q^2,s) = \frac{3g^2}{4\pi}\frac{p(q^2,s)^3}{m_\pi^2}, \tag{A2}$$

where $p(q^2, s)$ is the center of mass momentum of a ρ meson of mass $\sqrt{s}$ from the decay of an ω of mass $\sqrt{q^2}$ into the $\rho\pi$ system. The two-pion decay width of the ρ meson is given by

$$\Gamma_{\rho\to\pi\pi}(s) = \Gamma_0 \left(\frac{m_\rho}{\sqrt{s}}\right)^2 \left(\frac{s-4m_\pi^2}{m_\rho^2-4m_\pi^2}\right)^{\frac{3}{2}} \Theta(s-4m_\pi^2) \tag{A3}$$

with the on-shell decay width $\Gamma_0 = 149.2$ MeV.

The $\omega \to \pi\pi$ decay width is given by the very same expression but with the ρ on-shell width replaced by the corresponding decay width of the ω. From [67] we adopt the width for the semi-hadronic decay $\omega \to \pi^0\gamma$:

$$\Gamma_{\omega\to\pi^0\gamma}(q^2) = \frac{9}{24\pi}\left(\frac{d}{f_\pi}\right)^2 \left(\frac{q^2-m_\pi^2}{\sqrt{q^2}}\right)^3 \Theta(q^2-m_\pi^2) \tag{A4}$$

with $d \simeq 0.1$ and the pion decay constant $f_\pi = 92.4$ MeV. Neglecting the real part of the ω vacuum self energy, i. e. using the physical ω mass in the vacuum spectral function, we obtain the ω vacuum self energy:

$$\Pi(q^2) = -i\sqrt{q^2}\left(\Gamma_{\omega\to 3\pi}(q^2) + \Gamma_{\omega\to\pi^0\gamma}(q^2) + \Gamma_{\omega\to 2\pi}(q^2)\right) . \tag{A5}$$

APPENDIX B: LAGRANGIANS

As the coupling of the $N\omega$ channel to nucleon resonances is of special importance for the evaluation of the ω in-medium self energy, we give in the following the corresponding Lagrangians entering the K-matrix interaction potential:

$$\mathcal{L}_{\frac{1}{2}N\omega} = -\bar{u}_R \left\{ \begin{array}{c} 1 \\ -i\gamma_5 \end{array} \right\} \left(g_1\gamma_\mu - \frac{g_2}{2m_N}\sigma_{\mu\nu}\partial_\omega^\nu\right) u_N\omega^\mu + h.c. , \tag{B1}$$

$$\begin{aligned}\mathcal{L}_{\frac{3}{2}N\omega} &= -\bar{u}_R^\mu \left\{ \begin{array}{c} i\gamma_5 \\ 1 \end{array} \right\} \left(\frac{g_1}{2m_N}\gamma^\alpha + i\frac{g_2}{4m_N^2}\partial_N^\alpha + i\frac{g_3}{4m_N^2}\partial_\omega^\alpha\right) \left(\partial_\alpha^\omega g_{\mu\nu} - \partial_\mu^\omega g_{\alpha\nu}\right) u_N\omega^\nu \\ &\quad + h.c. ,\end{aligned} \tag{B2}$$

$$\begin{aligned}\mathcal{L}_{\frac{5}{2}N\omega} &= \bar{u}_R^{\mu\lambda} \left\{ \begin{array}{c} 1 \\ i\gamma_5 \end{array} \right\} \left(\frac{g_1}{4m_N^2}\gamma^\xi + i\frac{g_2}{8m_N^3}\partial_N^\xi + i\frac{g_3}{8m_N^3}\partial_\omega^\xi\right) \left(\partial_\xi^\omega g_{\mu\nu} - \partial_\mu^\omega g_{\xi\nu}\right) u_N\partial_\lambda^\omega\omega^\nu \\ &\quad + h.c. ,\end{aligned} \tag{B3}$$

where $h.c.$ denotes the hermitian conjugate. In all three cases the upper operator holds for positive and the lower one for negative parity resonances. In the spin-$\frac{3}{2}$ case the vertices are contracted with an off-shell projector that, for simplicity, is not displayed in Eq. (B2), see e. g. [55]. One should keep in mind, that the ωN forward scattering amplitude is not

obtained by just summing the individual tree-level contributions of the included resonances. In fact, by means of the Bethe-Salpeter equation rescattering effects are taken into account that turn out to play an important role already in the description of photon and pion induced ω production data on the nucleon.

APPENDIX C: SCATTERING LENGTH

The definition of the scattering length in the present paper differs from the definitions used in [58] and [45]. There a decomposition of the ωN helicity amplitudes with respect to the total angular momentum of the ωN system has been performed. In the present paper, however, we define the scattering length as done in [41], what is consistent with the evaluation of the self energy as given by Eqs. (2) and (7):

$$a_{\omega N} = \frac{m_N}{4\pi(m_N + m_\omega)} T_{\omega N}(q_0 = m_\omega), \tag{C1}$$

where $T_{\omega N}$ is the spin- and helicity-averaged ωN forward scattering amplitude at threshold:

$$T_{\omega N}(m_\omega) = \frac{1}{2}\left(T_{+1+\frac{1}{2}}(m_\omega) + T_{+1-\frac{1}{2}}(m_\omega)\right) = T_{0+\frac{1}{2}}(m_\omega). \tag{C2}$$

The lower indices stand for the ω and nucleon helicities. The amplitudes in the right-hand side of the Eq.(C2) are obtained from the partial wave decomposition [55]

$$\begin{aligned} T_\lambda(m_\omega) &= \frac{4\pi(m_N + m_\omega)}{p\, m_N} \sum_J \left(J + \frac{1}{2}\right) d^J_{\lambda\lambda'}(0) \left(T^{J+}_{\lambda'\lambda}(m_N + m_\omega) + T^{J-}_{\lambda'\lambda}(m_N + m_\omega)\right) \\ &= \frac{4\pi(m_N + m_\omega)}{p\, m_N} \left(T^{\frac{1}{2}^-}_{\lambda\lambda}(m_N + m_\omega) + 2T^{\frac{3}{2}^-}_{\lambda\lambda}(m_N + m_\omega)\right), \end{aligned} \tag{C3}$$

where p is the c.m. three-momentum and $\lambda = \lambda_\omega + \lambda_N$. Note, that only the $J^P = \frac{1}{2}^-$ and $J^P = \frac{3}{2}^-$ partial waves contribute close to the ωN threshold.

With the definition (C2), the classical interpretation of the scattering length similar as for spinless particles holds:

$$\sigma(\sqrt{s} = m_N + m_\omega) = \sigma^{\frac{1}{2}} + \sigma^{\frac{3}{2}} = 4\pi\left(3|a^{\frac{1}{2}^-}_{\omega N}|^2 + \frac{3}{2}|a^{\frac{3}{2}^-}_{\omega N}|^2\right) \tag{C4}$$

where σ is the usual spin- and helicity-averaged total ωN elastic cross section at threshold. With this definition the following formula for the on-shell mass shift applies:

$$\Delta m = -\frac{2\pi\rho_N}{m_\omega}\left(1 + \frac{m_\omega}{m_N}\right) \mathcal{R}e\ a_{\omega N} \tag{C5}$$

yielding a value of roughly 15 MeV. Note, however, that the shift of the ω peak in the spectral function is somewhat smaller since the real part of the self energy is reduced for q^2 values slightly above the ω pole mass, see Fig. 7.

---

[1] E. G. Drukarev and E. M. Levin, Nucl. Phys. **A511**, 679 (1990).

[2] T. D. Cohen, R. J. Furnstahl, and D. K. Griegel, Phys. Rev. **C45**, 1881 (1992).

[3] G.-Q. Li and C. M. Ko, Phys. Lett. **B338**, 118 (1994).

[4] R. Brockmann and W. Weise, Phys. Lett. **B367**, 40 (1996).

[5] G. E. Brown and M. Rho, Phys. Rev. Lett. **66**, 2720 (1991).

[6] T. Hatsuda and S. H. Lee, Phys. Rev. **C46**, 34 (1992).

[7] M. A. Shifman, A. I. Vainshtein, and V. I. Zakharov, Nucl. Phys. **B147**, 385, 448 (1979).

[8] A. I. Bochkarev and M. E. Shaposhnikov, Nucl. Phys. **B268**, 220 (1986).

[9] S. Zschocke, O. P. Pavlenko, and B. Kämpfer, Phys. Lett. **B562**, 57 (2003).

[10] R. Thomas, S. Zschocke, and B. Kämpfer, Phys. Rev. Lett. **95**, 232301 (2005), hep-ph/0510156.

[11] S. Leupold, Phys. Lett. **B616**, 203 (2005).

[12] F. Klingl, N. Kaiser, and W. Weise, Nucl. Phys. **A624**, 527 (1997).

[13] S. Leupold, W. Peters, and U. Mosel, Nucl. Phys. **A628**, 311 (1998).

[14] S. Leupold and M. Post, Nucl. Phys. **A747**, 425 (2005).

[15] G. Agakishiev et al. (CERES), Phys. Rev. Lett. **75**, 1272 (1995).

[16] G. Agakishiev et al. (CERES/NA45), Phys. Lett. **B422**, 405 (1998).

[17] B. Lenkeit et al. (CERES-Collaboration), Nucl. Phys. **A661**, 23 (1999).

[18] J. P. Wessels et al. (CERES/NA45), Nucl. Phys. **A715**, 262 (2003).

[19] M. Masera (HELIOS), Nucl. Phys. **A590**, 93c (1995).

[20] G.-Q. Li, C. M. Ko, and G. E. Brown, Phys. Rev. Lett. **75**, 4007 (1995).

[21] W. Cassing, W. Ehehalt, and C. M. Ko, Phys. Lett. **B363**, 35 (1995).

[22] W. Cassing, W. Ehehalt, and I. Kralik, Phys. Lett. **B377**, 5 (1996).

[23] E. L. Bratkovskaya and W. Cassing, Nucl. Phys. **A619**, 413 (1997).

[24] R. Arnaldi et al. (NA60), Phys. Rev. Lett. **96**, 162302 (2006), nucl-ex/0605007.

[25] U. Mosel, Prog. Part. Nucl. Phys. **42**, 163 (1999), nucl-th/9812067.

[26] T. Falter, J. Lehr, U. Mosel, P. Muehlich, and M. Post, Prog. Part. Nucl. Phys. **53**, 25 (2004).

[27] L. Alvarez-Ruso, T. Falter, U. Mosel, and P. Muehlich, Prog. Part. Nucl. Phys. **55**, 71 (2005).

[28] M. Post, S. Leupold, and U. Mosel, Nucl. Phys. **A741**, 81 (2004).

[29] K. Ozawa et al. (E325), Phys. Rev. Lett. **86**, 5019 (2001).

[30] T. Tabaru et al. (2006), nucl-ex/0603013.

[31] F. Sakuma et al. (2006), nucl-ex/0606029.

[32] D. Trnka et al. (CBELSA/TAPS), Phys. Rev. Lett. **94**, 192303 (2005).

[33] P. Muehlich, T. Falter, and U. Mosel, Eur. Phys. J. **A20**, 499 (2004).

[34] P. Muehlich, T. Falter, and U. Mosel (2004), nucl-th/0402039.

[35] C. Tur et al. (CLAS) (2004), private communication.

[36] M. Effenberger, E. L. Bratkovskaya, and U. Mosel, Phys. Rev. **C60**, 044614 (1999).

[37] R. Rapp and J. Wambach, Adv. Nucl. Phys. **25**, 1 (2000).

[38] V. Bernard and U. G. Meissner, Nucl. Phys. **A489**, 647 (1988).

[39] J. C. Caillon and J. Labarsouque, J. Phys. **G21**, 905 (1995).

[40] B. Friman, Acta Phys. Polon. **B29**, 3195 (1998).

[41] F. Klingl, T. Waas, and W. Weise, Nucl. Phys. **A650**, 299 (1999).

[42] K. Saito, K. Tsushima, A. W. Thomas, and A. G. Williams, Phys. Lett. **B433**, 243 (1998).

[43] K. Saito, K. Tsushima, D. H. Lu, and A. W. Thomas, Phys. Rev. **C59**, 1203 (1999).

[44] M. Post and U. Mosel, Nucl. Phys. **A688**, 808 (2001).

[45] M. F. M. Lutz, G. Wolf, and B. Friman, Nucl. Phys. **A706**, 431 (2002).

[46] A. K. Dutt-Mazumder, Nucl. Phys. **A713**, 119 (2003).

[47] T. Renk and A. Mishra, Phys. Rev. **C69**, 054905 (2004).

[48] A. T. Martell and P. J. Ellis, Phys. Rev. **C69**, 065206 (2004).

[49] F. Riek and J. Knoll, Nucl. Phys. **A740**, 287 (2004).

[50] A. K. Dutt-Mazumder, R. Hofmann, and M. Pospelov, Phys. Rev. **C63**, 015204 (2001).

[51] B. Steinmueller and S. Leupold, Nucl. Phys. **A** (2006), accepted for publication, hep-ph/0604054.

[52] P. Muehlich et al., Phys. Rev. **C67**, 024605 (2003).

[53] T. Feuster and U. Mosel, Phys. Rev. **C58**, 457 (1998).

[54] T. Feuster and U. Mosel, Phys. Rev. **C59**, 460 (1999).

[55] G. Penner and U. Mosel, Phys. Rev. **C66**, 055211 (2002).

[56] G. Penner and U. Mosel, Phys. Rev. **C66**, 055212 (2002).

[57] V. Shklyar, G. Penner, and U. Mosel, Eur. Phys. J. **A21**, 445 (2004).

[58] V. Shklyar, H. Lenske, U. Mosel, and G. Penner, Phys. Rev. **C71**, 055206 (2005).

[59] C. B. Dover, J. Hüfner, and R. H. Lemmer, Ann. Phys. **66**, 248 (1971).

[60] M. E. Peskin and D. V. Schroeder, *An Introduction to Quantum Field Theory* (Perseus, Cambridge, Massachusetts, 1995).

[61] G. Penner, PhD thesis (in English), Giessen, available via http://theorie.physik.uni-giessen.de (2002).

[62] L. M. Barkov et al., JETP Lett. **46**, 164 (1987).

[63] S. I. Dolinsky et al., Phys. Rept. **202**, 99 (1991).

[64] P. Muhlich and U. Mosel, Nucl. Phys. A (2006).

[65] S. Eidelman et al. (Particle Data Group), Phys. Lett. **B592**, 1 (2004).

[66] B. Friman and H. J. Pirner, Nucl. Phys. **A617**, 496 (1997), nucl-th/9701016.

[67] F. Klingl, N. Kaiser, and W. Weise, Z. Phys. **A356**, 193 (1996).